

Equation of State Model for the $\gamma - \alpha$ Transition in Ce

C. W. Greeff¹, S. D. Crockett¹ and K. G. Honnell¹

¹ *Los Alamos National Laboratory, Los Alamos, NM 87545*

Abstract. The element Ce exhibits an isostructural $\gamma - \alpha$ phase transition with a 15% volume change at room temperature. The phase boundary ends in a critical point at 1.5 GPa and 480 K. We describe a model for the equation of state of Ce in the $\gamma - \alpha$ transition region. The model is based on the idea, supported by modern many-body calculations, of a continuously varying degree of localization of the $4f$ electrons as a function of compression. The functional forms used are motivated by many-body calculations, with parameters determined by experiments, resulting in a physics-based empirical EOS. In the large-volume γ phase, degeneracy of the $j = 5/2$ state of the localized $4f$ electron makes a large contribution to the entropy. Rapid variation of the thermal electronic free energy with volume leads to unusually large electronic contributions to the pressure and thermodynamic Grüneisen parameter. The static lattice energy has two local minima, with the α -like minimum lower than the γ -like one by 6.3 meV/atom.

INTRODUCTION

The element Ce exhibits many interesting phenomena. Chief among these is the isostructural $\gamma - \alpha$ phase transition. This transition involves a discontinuity in volume as a function of pressure, but no change of crystal structure, both phases being fcc. The volume discontinuity decreases with increasing temperature, and vanishes at a critical point at $T = 480$ K and $P = 1.5$ GPa. Having a volume change but no symmetry change, and ending in a critical point, the transition is analogous to the liquid-vapor transition.

The $\gamma - \alpha$ transition has large volume and entropy changes of 15% and $1.5k_B$ /atom, respectively, at room temperature [1, 3]. The phase diagram in this region is shown in Fig. 1. In addition to the fcc γ and α phases, at ambient pressure and just below room temperature, there is the dhcp structured β phase. At high temperature, there is a bcc δ phase. The melting curve is anomalous with $dT_{\text{melt}}/dP < 0$ at low pressure. The melting temperature reaches a minimum near 3.2 GPa, and increases at higher pressures. Other phases enter beyond the range of the plot. These show large history dependence and other anomalies, resulting in significant uncertainty regarding the equilibrium phase diagram at high pressures [2, 4]. Under dynamic compression, the large volume collapse of the $\gamma - \alpha$ transition leads to strong shock heating, contributing to the unusually low shock melting pressure of 10 GPa [5]. In addition, the bulk modulus of the γ phase decreases on compression, leading to anomalous spreading of compression waves [6].

The existence of the isostructural transition in Ce has its origins in the behavior of its $4f$ electrons. Ce belongs to the lanthanide series where the $4f$ shell is partially full, and it has a nominal configuration of $[\text{Xe}]4f^15d^16s^2$. The $4f$ atomic state is energetically in the valence, but spatially localized. This results in narrow energy bands in the solid, so that the on-site Coulomb repulsion is larger than the bandwidth. Electron correlation effects are significant, and the mean-field picture of Bloch band states breaks down. Compression increases the bandwidth, effectively reducing the strength of correlations. In the strong interaction limit, the $4f$ electrons are localized on atomic sites. We show below that the localized $4f$ limit gives a good description of the thermodynamic properties of the large-volume γ phase. The $\gamma - \alpha$ transition is associated with a change from localized to itinerant behavior of the $4f$ electrons.

The earliest equation of state model for the transition is due to Aptekar and Ponyatovskiy [7], who considered the transition to be due to a change of valence of Ce ions. They constructed a pseudo-alloy model, picturing two types of Ce atoms, with a concentration-dependent configuration entropy,

$$S_{\text{conf}} = Nk_B [x \ln(x) + (1 - x) \ln(1 - x)] \quad (1)$$

corresponding to the number of arrangements of the two types of atoms, where x is the concentration of α -like atoms. Later, Johansson *et al.* [8] formulated a model based on the picture of a Mott transition between localized and delocalized $4f$ electrons. They incorporated a magnetic entropy in the localized, γ -like state, which is included in our

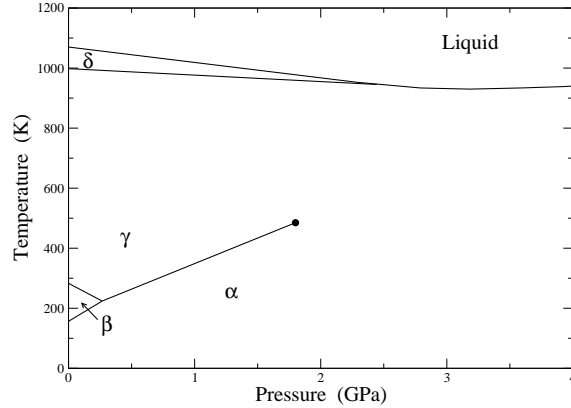


FIGURE 1. Phase diagram of Ce at low pressure [1] and [2]. The γ and α phases have the fcc structure. Their phase boundary ends at a critical point marked by the dot. The β phase has the dhcp structure, and δ is bcc.

model as well. Similar to Aptekar and Ponyatovskiy, they adopt a pseudo-alloy approach, with the same configuration entropy. More recently, Elkin *et al.* have developed an equation of state for several phases of Ce [9], which describes a wide range of data well. Their treatment of the $\gamma - \alpha$ transition also invokes a pseudo-alloy picture, similar to that of Aptekar and Ponyatovskiy. They consider the two atom types in the pseudo-alloy to be in pressure equilibrium.

The present model is motivated by both practical and theoretical considerations. We wish to have a parameterized equation of state for the $\gamma - \alpha$ region that is compatible with our existing framework for generating wide-ranging multi-phase equations of state [10]. We would like to be able to use the analytic formulation of the model in-line in hydrodynamic simulations which include phase transition kinetics [11]. The model of Elkin *et al.* [9] is difficult to use in this setting because of the requirement of pressure equilibrium, which introduces an additional layer of transformation between volume and pressure as the independent variable. Theoretically, the pseudo-alloy picture is dubious. There is no way to assign an individual atom as localized or itinerant, and the meaning of the configuration entropy S_{conf} is unclear. Here we formulate a model for the Helmholtz free energy of fcc Ce in the form of a sum of static lattice energy and ionic and electronic excitation contributions,

$$F(V, T) = \phi(V) + F_{\text{ion}}(V, T) + F_{\text{el}}(V, T). \quad (2)$$

Both the static lattice energy ϕ and the electronic excitation terms have unusual functional forms related to the delocalization of the $4f$ electrons under compression. We use modern many-body calculations to guide the functional forms of the models [12, 13, 14]. These show a rapid, but continuous increase in the $4f$ spectral weight at the Fermi surface, and the strength of the $4f$ quasiparticle pole under compression. Our model represents this with a continuous transition from a localized to Fermi-liquid behavior. The many-body calculations also show a non-convex variation of $\phi(V)$, and our model incorporates this.

EOS MODEL

Electronic Excitation

Standard equation of state models for metals include the phonon contributions through an effective Debye model, and an electronic term of the form $F_{\text{el}} = -\Gamma T^2$, where Γ is the Sommerfeld coefficient, which is proportional to the electronic density of states [19]. Good estimates for these parameters are available from measurements for γ Ce. The phonon dispersion curves were measured by Stassis *et al.* [20]. From these data, the logarithmic moment, $\theta_0 = hv_0/k_B$, which determines the entropy in the high temperature limit, is 116 K. Using this as the effective Debye temperature, and the γ phase Sommerfeld coefficient $\Gamma = 6.2$ mJ/mol K² [17], we obtain the red dashed curves in the upper panel of Fig. 2. It can be seen that the entropy obtained from these parameters is substantially smaller than the experimental

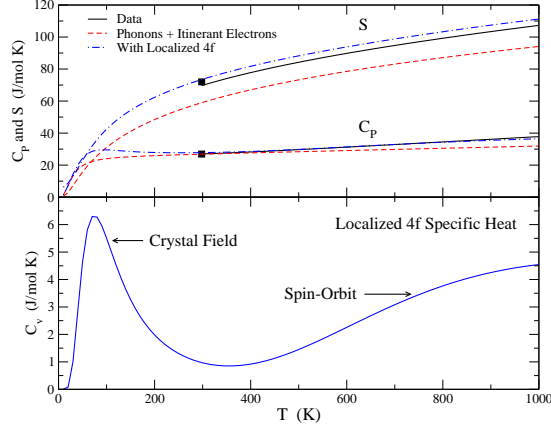


FIGURE 2. Entropy and specific heat of γ Ce. Solid black curve is data from Konings and Beneš [15] and black squares are from Gschneidner [16]. Red dashed curves are phonon and itinerant electron contributions only, blue dot-dash curves also include localized 4f electrons. Lower panel shows the contribution of the localized 4f electrons to the specific heat.

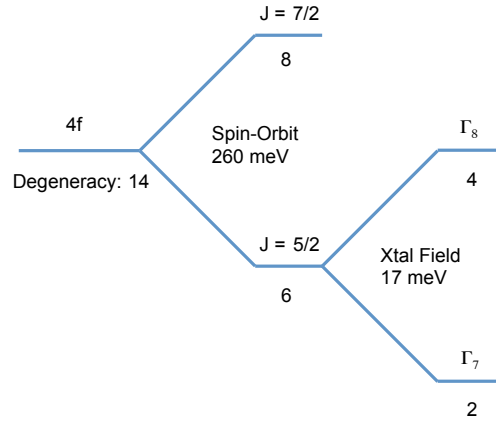


FIGURE 3. Energy levels of a 4f electron in γ Ce [17, 18]. Numbers below horizontal lines give degeneracies.

entropy [16, 15]. The difference is $12 \text{ J/mol K} = 1.4 k_B/\text{atom}$, which is similar to the $\gamma - \alpha$ entropy change. The entropy can be increased by raising Γ , but that also increases the specific heat, in conflict with data. The only way to increase the entropy within this model, without increasing the high temperature specific heat, is to decrease the Debye temperature. To obtain agreement with data, we must set θ_D to 80 K. A range of 115-137 K is given for various measurements aggregated by Lipp *et al.* [21], so 80 K is well outside the range of experimental data.

To account for the measured entropy of γ Ce, we must include the effects of the localized 4f electron. The energy levels of the γ Ce 4f electron are shown in Fig. 3. Starting from a 14-fold orbital and spin degeneracy, spin orbit coupling splits these into a 6-fold degenerate $j = 5/2$ state and an 8-fold degenerate $j = 7/2$ state, with the latter lying 260 meV above the former [18]. Crystal fields further split the $j = 5/2$ state into 2-fold degenerate Γ_7 and 4-fold Γ_8 representations, which are separated by 17 meV [17]. Spins on different atomic sites are correlated at a still lower energy scale. For instance β Ce undergoes a magnetic ordering transition at ~ 12 K, with a corresponding energy scale ~ 1 meV [22]. Since we are concerned with properties near room temperature and above, these energies are negligible, and we can regard the atomic moments as independent. Then the thermodynamic functions associated with the localized 4f electrons are obtained straightforwardly from the partition function. The Helmholtz free energy is $F_{\text{loc}} = -Nk_B T \ln Z_{\text{loc}}$, where $Z_{\text{loc}} = \sum_i g_i \exp(-\beta \epsilon_i)$, and g_i and ϵ_i are the degeneracies and energies in Fig. 3.

Including this contribution leads to the blue dash-dot curves in Fig. 2, which are in much better agreement with

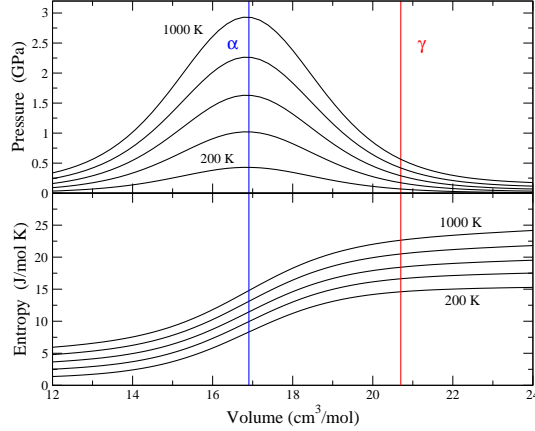


FIGURE 4. Entropy and pressure from the electron free energy F_{el} given in Eq. (5).

experiment. The lower panel shows the contribution of F_{loc} to the specific heat. The crystal field splitting leads to a peak at low temperature, below the stability of the γ phase. In the temperature range of interest, essentially from room temperature up, the main effect of the localized $4f$ electrons is to increase the entropy by $Nk_B \ln(6)$, where 6 is the combined number of $j = 5/2$ states. Excitations to the $j = 7/2$ states contribute an enhancement of the high temperature specific heat, which also improves agreement with data. The entropy from our complete model, described below, is in somewhat better agreement with data because the $4f$ electrons are not completely localized at the ambient γ phase volume.

To complete the electronic free energy model, we must incorporate a volume dependence such that under compression, the free energy changes over to that of a normal Fermi liquid. Our model is motivated by DMFT calculations that show a smooth buildup of $4f$ spectral weight at the Fermi surface [12, 13]. The entropy curves shown in Fig. 2 of Bieder and Amadon [13], show a component at large volume that is nearly temperature independent above 300 K, and is close to $S/Nk_B = \ln(14)$. Their calculations do not include spin-orbit coupling, so this corresponds to the $\ln(6)$ in our model associated with the local $4f$ moment. At small volumes, their entropy is close to linear in T , as expected for a normal Fermi liquid. We therefore formulate our electron thermal model for the $4f$ electrons as,

$$F_f(V, T) = h(V)F_{loc}(T) - [1 - h(V)] \frac{1}{2} \Gamma_f T^2 \quad (3)$$

where h is a switch function going from one at large volume to zero at small volume.

$$h(V) = e^x / (e^x + 1) \quad (4)$$

where $x = (V - V_{loc}) / \Delta V_{loc}$. The parameters V_{loc} and ΔV_{loc} control the location and width of the transition, respectively. We have chosen to make Γ_f volume independent and to make h a function of V alone in order to limit the number of parameters in the model. Initial values of the parameters V_{loc} and ΔV_{loc} were chosen by matching the 600 K isotherm of the DMFT calculations in Fig. 2 of Bieder and Amadon [13]. These were then fine-tuned to match data on the phase diagram. The assumption that h depends only on V is somewhat limiting. Matching the phase diagram tends to favor smaller values of V_{loc} , which correspond to higher temperatures in the DMFT calculations.

The complete electron model includes the other conduction electrons of s , p , and d -like character. These are represented together with a separate volume-dependent Sommerfeld coefficient,

$$F_{el}(V, T) = F_f(V, T) - \frac{1}{2} \Gamma_{spd}(V) T^2 \quad (5)$$

where the volume dependence is given by, $\Gamma_{spd}(V) = \Gamma_{0,spd}(V/V_{0,spd})^\kappa$.

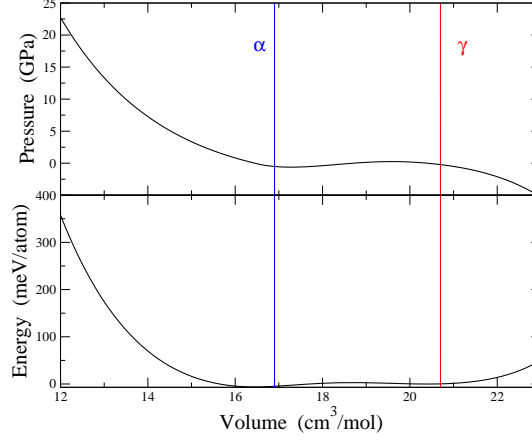


FIGURE 5. Static lattice energy and corresponding pressure.

In addition to the energy levels and degeneracies listed in Fig. 3 for the localized $4f$ electrons, the following parameters are used,

$$\begin{aligned}
 \Gamma_{0\,spd} &= 6.12 \text{ mJ/mol K}^2 \\
 \kappa &= 1.0 \\
 \Gamma_f &= 2.13 \text{ mJ/mol K}^2 \\
 V_{\text{loc}} &= 16.85 \text{ cm}^3/\text{mol} \\
 \Delta V_{\text{loc}} &= 1.20 \text{ cm}^3/\text{mol}
 \end{aligned} \tag{6}$$

Figure 4 shows the entropy and pressure corresponding to the electronic free energy, Eq. (5). At large volumes, the entropy rises quickly to the $Nk_B \ln(6)$ value from the local moments. The transition volume from localized to itinerant $4f$ electrons is close to the ambient pressure α phase volume. At small volumes, the entropy is linear in T , with coefficient $\Gamma_f + \Gamma_{spd}$. The rapid variation of the entropy with volume is accompanied by a peak in the electronic contribution to the pressure, in accord with the thermodynamic identity $(\partial S/\partial V)_T = (\partial P/\partial T)_V$. The electron-thermal pressure is exceptionally large in the transition region, and is comparable to the critical pressure. The thermodynamic Grüneisen parameter $\gamma_{\text{th}} = V(\partial P/\partial E)_V$ is observed to show a peak for volumes near the $\gamma - \alpha$ phase transition [1]. In the present model, this peak is attributed to thermal electronic excitations, rather than lattice vibrations.

Static Lattice Energy

Our static lattice energy is modeled on results from many-body calculations that show non-convex shape of $\phi(V)$, leading to double tangents. For instance, Fig. 1 of Tian *et al.* [14] shows results of LDA + Gutzwiller calculations on $\phi(V)$ for different values of the on-site coulomb interaction parameter U . These show “normal” regions with $e^2\phi/dV^2 > 0$ separated by an anomalous region with negative curvature.

We therefore formulate our static lattice energy as follows. We define a γ -like region at larger volumes, and an α -like one at small volumes, each of which is described by the Vinet form.

$$\phi(V) = \phi_* + \frac{4V_*B_*}{(B'_* - 1)^2} \left[1 - (1 + X)e^{-X} \right] \tag{7}$$

$$X = \frac{3}{2}(B'_* - 1) \left[(V/V_*)^{1/3} - 1 \right] \tag{8}$$

The quantities ϕ_* , V_* , B_* , and B'_* are the energy, volume, bulk modulus, and its pressure derivative evaluated at the minimum of the corresponding segment. The ambient density and bulk modulus are primarily controlled by the parameters of the γ -like Vinet curve. The α -like Vinet curve controls the cold properties on the high pressure side of

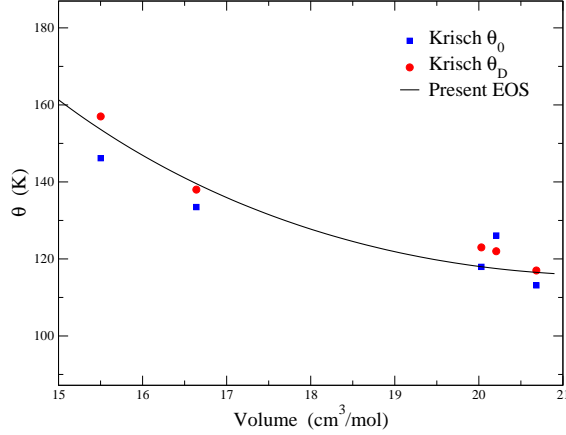


FIGURE 6. Effective Debye temperatures as functions of the volume. Squares are θ_0 determined by integrating the density of states from Krisch *et al.* [24] and circles are their reported values based on Debye-Waller factors. Solid black curve is the present model.

the transition. It gives the dominant contribution to the room temperature isotherm at high pressure. We have used room temperature data to 208 GPa [23] to determine parameters for the α -like Vinet curve. This includes the α'' and bct phases as well as α , so our high pressure ϕ incorporates these phases in a smoothed way.

We specify the static lattice transition pressure P_{tr} as an input. This is approximately the $T = 0$ transition pressure, but because the zero-point vibration energy is included in F_{ion} , the two are not exactly the same. We solve for the volumes V_1 and V_2 where the pressure is equal to P_{tr} on the γ and α -like Vinet curves, respectively. For $V > V_1$, we use the γ -like Vinet curve, and for $V < V_2$ the α -like curve. In between, we use a polynomial in V . The coefficients are chosen so that there is continuity of the pressure and its volume derivative at V_1 and V_2 , and so that the enthalpies $H = E + PV$ are equal at these two volumes. This is the condition of phase equilibrium. These conditions require a fifth order polynomial. The current set of parameters are,

$$\begin{aligned}
 V_*^\gamma &= 20.4 \text{ cm}^3/\text{mol} \\
 B_*^\gamma &= 13.0 \text{ GPa} \\
 B_*^{\gamma'} &= -20 \\
 V_*^\alpha &= 16.54 \text{ cm}^3/\text{mol} \\
 B_*^\alpha &= 27.0 \text{ GPa} \\
 B_*^{\alpha'} &= 6.5 \\
 P_{tr} &= -0.15 \text{ GPa}
 \end{aligned} \tag{9}$$

The resulting $\phi(V)$ and its corresponding pressure are shown in Fig. 5. The γ phase minimum is higher than the α phase by 6.3 meV/atom. The local maximum between the two is 2.9 meV/atom above the γ minimum. This conveys a sense of the small energy scales at work in the phase transition. Our empirical energy curve is similar to Tian's [14] result for $U = 4.5$ eV. However, using other criteria, they selected $U = 4.0$ eV as the best value, which gives a much larger energy difference between α and γ . This indicates that some fine-tuning of U is likely to be needed to get a qualitatively correct phase diagram in correlated electron calculations.

Ion Motion

The ion motion free energy is simply the Debye model with a volume-dependent effective Debye temperature $\theta(V)$. The dependence of θ on V is prescribed through the phonon Grüneisen parameter $\gamma^{ph} = -d \ln \theta / d \ln V$ whose volume dependence we take to be,

$$\gamma(V) = \gamma^\infty + A \left(\frac{V}{V_0} \right) + B \left(\frac{V}{V_0} \right)^2, \tag{10}$$

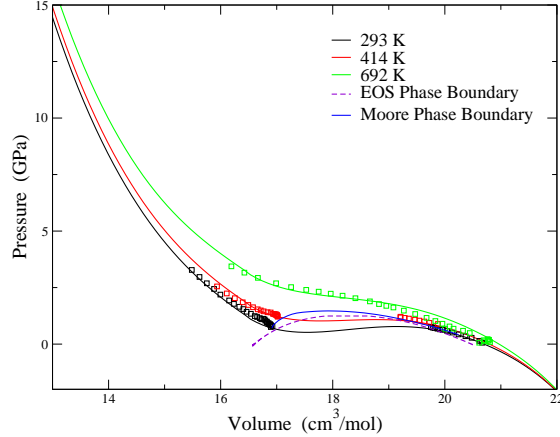


FIGURE 7. Isotherms and $\gamma - \alpha$ phase boundary. Symbols are data from Lipp *et al.* [1]. Solid blue phase boundary is from Moore *et al.* [25].

where γ^∞ , A , and B are material parameters. We specify A and B by giving $\gamma(V_0)$ and $q = d \ln(\gamma)/d \ln(V)|_{V_0}$.

Krisch *et al.* present measurements of the phonon dispersion curves under pressure. From their Debye-Waller factors they inferred the volume dependence of an effective Debye temperature $\theta_D(V)$. They also give graphs of the density of states $g(\omega)$, from which we could determine moments. In particular, the logarithmic moment

$$\omega_0 = e^{1/3} \exp \left[\int d\omega g(\omega) \ln \omega \right] \quad (11)$$

is of interest because it determines the entropy in the high temperature (classical) limit, and $\theta_0 = \hbar\omega_0/k_B$ is often used as an effective Debye temperature. Figure 6 shows these two effective Debye temperatures as functions of volume, along with the present model, which follows equation 10. The two moments follow generally the same trends and our model is between them. The experimental moments are not smooth enough to usefully determine $\gamma_{\text{ph}} = d \ln(\theta)/d \ln(V)$ by numerical differentiation. Some general features are supported by the data. The phonon Grüneisen parameter γ_{ph} is small at ambient conditions, and through the transition region. It increases under compression, in contrast to the usual trend. Our model uses the following parameters for the vibrational free energy,

$$\begin{aligned} V_0 &= 20.67 \text{ cm}^3/\text{mol} \\ \theta(V_0) &= 116.5 \text{ K} \\ \gamma(V_0) &= 0.3 \\ q &= -20 \\ \gamma^\infty &= 2/3 \end{aligned} \quad (12)$$

The large negative value of q is unusual, reflecting the anomalous increase of γ_{ph} under compression.

RESULTS

Figure 7 shows some isotherms in the $\gamma - \alpha$ transition region, along with the phase boundary. The phase boundary for the EOS is obtained by solving $P(V_\gamma, T) = P(V_\alpha, T)$ simultaneously with $G(V_\gamma, T) = G(V_\alpha, T)$ where $P = -\partial F/\partial V$ is the pressure, and $G = F + PV$ is the Gibbs free energy. The $P(V)$ compression data is obtained in diamond anvil cell experiments by Lipp *et al.* [1]. The experimental phase boundary is from Moore *et al.* [25]. The isotherms are generally matched well by the model, both their volume and temperature dependence. Figure 8 shows the $\gamma - \alpha$ phase boundary in the T, P plane with data [2, 1]. The model's critical temperature is in good agreement with data. The phase boundary is in overall good agreement with data, both in the P, V and T, P planes, except that the transition pressures are too low by about 0.2 GPa.

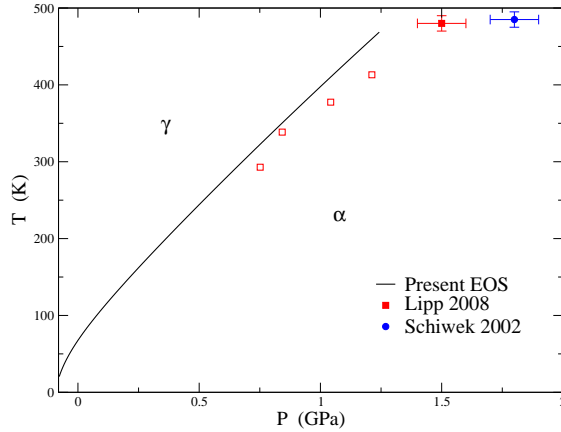


FIGURE 8. The $\gamma - \alpha$ phase boundary with data [1, 2] Filled symbols are measurements of the critical point.

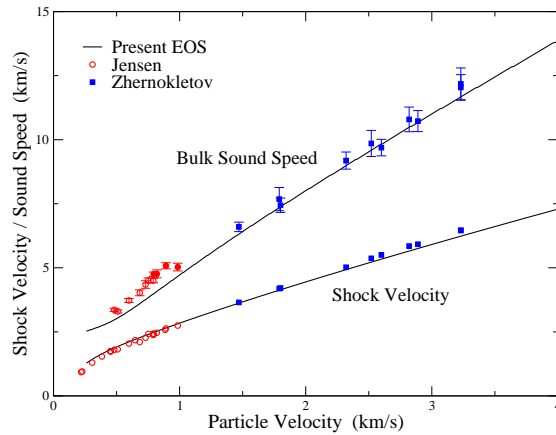


FIGURE 9. Hugoniot and bulk sound speed of shocked Ce. Data from Jensen and Cherne [6] and Zhernokletov *et al.* [26].

Figure 9 shows the Hugoniot and bulk sound speed from the model compared with data [6, 26]. While the model refers to the solid $\gamma - \alpha$ phases, the data above $U_p \sim 0.8$ km/s is in the liquid. In spite of this, the high pressure Hugoniot is in fair agreement with the data. Because we have used data from high pressure phase to parameterize our α -like static lattice pressure, this agreement shows that the EOS of the liquid is similar to that of the high pressure solid phases. Inclusion of a distinct liquid phase should move the Hugoniot higher, in the right direction to improve agreement with data. The sound speeds at low pressure are systematically low. The peak of the sound speed near melting was not reproduced with any values of the parameters we tried.

CONCLUSIONS

We have formulated a model for the free energy of fcc Ce in the region of the $\alpha - \gamma$ isostructural phase transition. The pseudo-alloy picture [7, 8, 9] is not invoked, and instead the $4f$ electrons are considered to transition rapidly but smoothly from localized to de-localized under compression. This de-localization is represented by a non-covex static lattice energy and an unusual form for the electronic excitation free energy. Electronic excitations account for almost all of the entropy change at the phase boundary, and contribute substantially to the pressure, owing to the rapid

variation of the electronic spectrum with volume.

The model has correct qualitative behavior and describes a variety of data rather well. Improvements should be possible by further refinement of the parameters. The present parameters were obtained from estimates based on data and theoretical calculations, which were then partially optimized by hand. Automatic optimization will be needed to systematically improve them. A potentially significant physical improvement to the model would be to generalize the transition from localized to de-localized $4f$ electrons, as governed by equations 3 and 4, to depend on volume and temperature, rather than volume alone. Entropy curves from microscopic calculations indicate [12, 13] the need for explicit temperature dependence. A tractable way to do this might be to follow the method of reference [1] by introducing a scaled temperature, $h(V, T) = f(T/T_K(V))$, where T_K is the Kondo temperature.

ACKNOWLEDGMENTS

We gratefully acknowledge support from Advanced Simulation and Computing at LANL which is operated by LANS, LLC for the NNSA of the U.S. DOE under Contract No. DE-AC52-06NA25396, and helpful discussions with John Wills and Frank Cherne.

REFERENCES

- [1] M. J. Lipp, D. Jackson, H. Cynn, C. Aracne, W. J. Evans, and A. K. McMahan, *Phys. Rev. Lett.* **101**, p. 165703 (2008).
- [2] A. Schiwiek, F. Porsch, and W. B. Holzapfel, *High Pressure Research* **22**, 407–410 (2002), <http://dx.doi.org/10.1080/08957950212799>.
- [3] B. Amadon, S. Biermann, A. Georges, and F. Aryasetiawan, *Phys. Rev. Lett.* **96**, p. 066402 (2006).
- [4] O. B. Tsiok and L. G. Khvostantsev, *Journal of Experimental and Theoretical Physics* **93**, 1245–1249 (2001).
- [5] B. Jensen, F. Cherne, J. Cooley, M. Zhernokletov, and A. Kovalev, *Physical Review B* **81**, p. 214109 (2010).
- [6] B. Jensen and F. Cherne, *Journal of Applied Physics* **112**, p. 013515 (2012).
- [7] I. L. Aptekar and Y. G. Ponyatovskiy, *Fiz. Metal. Metalloved.* **25**, 777–786 (1968).
- [8] B. Johansson, I. A. Abrikosov, M. Aldén, A. V. Ruban, and H. L. Skriver, *Phys. Rev. Lett.* **74**, 2335–2338 (1995).
- [9] V. M. Elkin, V. N. Mikhaylov, A. V. Petrovtsev, and F. J. Cherne, *Phys. Rev. B* **84**, p. 094120 (2011).
- [10] E. D. Chisolm, C. W. Greeff, and D. C. George, “Constructing explicit multiphase equations of state with opensesame,” *Tech. Rep. LA-UR-05-9413* (Los Alamos National Laboratory).
- [11] C. W. Greeff, *Journal of Dynamic Behavior of Materials* **2**, 452–459 (2016).
- [12] A. K. McMahan, K. Held, and R. T. Scalettar, *Phys. Rev. B* **67**, p. 075108 (2003).
- [13] J. Bieder and B. Amadon, *Phys. Rev. B* **89**, p. 195132 (2014).
- [14] M.-F. Tian, H.-F. Song, H.-F. Liu, C. Wang, Z. Fang, and X. Dai, *Phys. Rev. B* **91**, p. 125148 (2015).
- [15] R. J. M. Konings and O. Beneš, *Journal of Physical and Chemical Reference Data* **39**, p. 043102 (2010), <http://aip.scitation.org/doi/pdf/10.1063/1.3474238>.
- [16] K. A. Gschneidner, *Bulletin of Alloy Phase Diagrams* **11**, 216–224 (1990).
- [17] M. E. Manley, R. J. McQueeney, B. Fultz, R. Osborn, G. H. Kwei, and P. D. Bogdanoff, *Phys. Rev. B* **65**, p. 144111 (2002).
- [18] S. Arajs and R. Colvin, *Journal of the Less Common Metals* **4**, 159 – 168 (1962).
- [19] C. W. Greeff and M. J. Graf, *Phys. Rev. B* **69**FEB (2004), 10.1103/PhysRevB.69.054107.
- [20] C. Stassis, T. Gould, O. D. McMasters, K. A. Gschneidner, and R. M. Nicklow, *Phys. Rev. B* **19**, 5746–5753 (1979).
- [21] M. J. Lipp, Y. Kono, Z. Jenei, H. Cynn, C. Aracne-Ruddle, C. Park, C. Kenney-Benson, and W. J. Evans, *Journal of Physics: Condensed Matter* **25**, p. 345401 (2013).
- [22] J. M. Lock, *Proceedings of the Physical Society, Section B* **70**, p. 566 (1957).
- [23] Y. K. Vohra, S. L. Beaver, J. Akella, C. A. Ruddle, and S. T. Weir, *Journal of Applied Physics* **85**, 2451–2453 (1999), <http://dx.doi.org/10.1063/1.369566>.
- [24] M. Krisch, D. L. Farber, R. Xu, D. Antonangeli, C. M. Aracne, A. Beraud, T.-C. Chiang, J. Zarestky, D. Y. Kim, E. I. Isaev, R. Ahuja, and B. Johansson, *Proceedings of the National Academy of Sciences* **108**, 9342–9345 (2011), <http://www.pnas.org/content/108/23/9342.full.pdf>.
- [25] K. Moore, L. Belhadi, F. Decremps, D. Farber, J. Bradley, F. Occelli, M. Gauthier, A. Polian, and C. Aracne-Ruddle, *Acta Materialia* **59**, 6007 – 6016 (2011).
- [26] M. V. Zhernokletov, A. E. Kovalev, V. V. Komissarov, M. G. Novikov, M. A. Zocher, and F. J. Cherne, *Journal of Physics: Conference Series* **121**, p. 072003 (2008).